

A Coumarin Embedded Highly Sensitive Nitric Oxide Fluorescent Sensor: Kinetic Assay and Bio-imaging Applications

Debjani Maiti^a, Abu Saleh Musha Islam^a, Mihir Sasmal^a, Ananya Dutta^a, Atul Katarkar^b, and Mahammad Ali ^{*a,c}

^a Department of Chemistry, Jadavpur University, Kolkata 700 032, India; E-mail: m_ali2062@yahoo.com, vc_au@aliah.ac.in

^b Department of Biochemistry, University of Lausanne, Ch. des Boveresses 155, 1066 Epalinges, Switzerland

^c Vice-Chancellor, Aliah University, II-A/27, Action Area II, Newtown, Action Area II, Kolkata, West Bengal 700160; vc_au@aliah.ac.in

No.	Content	Figure No.
1.	¹ H NMR spectrum of (L ¹) in DMSO- <i>d</i> ₆ .	Fig.S1.
2.	¹³ C NMR spectrum of (L ¹) in DMSO- <i>d</i> ₆ .	Fig. S2.
3.	¹ H NMR spectrum of BCM in DMSO- <i>d</i> ₆ .	Fig.S3.
4.	¹³ C NMR spectrum of BCM in DMSO- <i>d</i> ₆	Fig. S4.
5.	Mass spectrum of BCM.	Fig. S5.
6.	IR spectrum of BCM	Fig. S6.
7.	Mass spectrum of BCM-NO	Fig. S7.
8.	¹ H NMR spectrum of BCM-NO .	Fig. S8
9.	IR spectrum of BCM-NO	Fig.S9
10.	Mass spectrum of BCM-NO after long time (acid product)	Fig.S10
11.	¹ H NMR spectrum of BCM-NO after long time (acid product)	Fig. S11
12.	(a)Time-dependent fluorescence response and (b) corresponding growth curve for [BCM] = 5.0 μM and [NO] 5 μM at 15 °C.	Fig. S12.
13.	Plot of log(<i>k</i> _{obs}) vs. log [NO].	Fig.S13.
14.	Plot of log(<i>k</i> _{obs}) vs. log [BCM].	Fig.S14
15.	LOD of BCM + NO.	Fig.S15
16.	(a)Bar chart illustrating fluorescence response of BCM to different cations at 470 nm (λ _{ex} = 410 nm) in HEPES buffer pH 7.0; BCM = 20 μM, X ⁿ⁺ = 50 μM. (b) spectral responses.	Fig.S16
17.	Bar chart illustrating fluorescence response of BCM at 470 nm (λ _{ex} = 410 nm) towards NO in presence of different cations in HEPES buffer pH 7.0; BCM = 20 μM, X ⁿ⁺ = 50 μM.	Fig.S17
18.	(a)Bar chart illustrating fluorescence response of BCM to different cations at 470 nm (λ _{ex} = 410 nm) in HEPES buffer	Fig. S18

	pH 7.0; BCM = 20 μ M, X ⁿ⁻ = 50 μ M. (b) spectral responses.	
19.	Bar chart illustrating fluorescence response of BCM at 470 nm ($\lambda_{\text{ex}} = 410$ nm) towards NO in presence of different anions in HEPES buffer pH 7.0; BCM = 20 μ M, X ⁿ⁻ = 50 μ M.	Fig.S19
20.	Frontier molecular orbitals of BCM and BCM-NO in UV-vis absorption.	Fig. S20.
21.	UV titration of BCM in presence of NO	Fig. S21.
22.	Some selected geometrical parameters (bond lengths and bond angles) of BCM in ground state calculated at B3LYP/6-31G (d) Levels.	Table S1.
23.	Some selected geometrical parameters (bond lengths and bond angles) of BCM-NO in ground state calculated at B3LYP/6-31G (d) Levels.	Table S2.
24.	Vertical excitation energy and oscillator strength (f_{cal}) of low-lying excited singlet states obtained from TDDFT// B3LYP/6-31G(d,p) calculations of BCM which is matched with the experimental one.	Table S3.
25.	Vertical excitation energy and oscillator strength (f_{cal}) of low-lying excited singlet states obtained from TDDFT// B3LYP/6-31G(d,p) calculations of BCM-NO which is matched with the experimental one.	Table S4.
26.	Comparison table of some nitric oxide probes	Table S5.

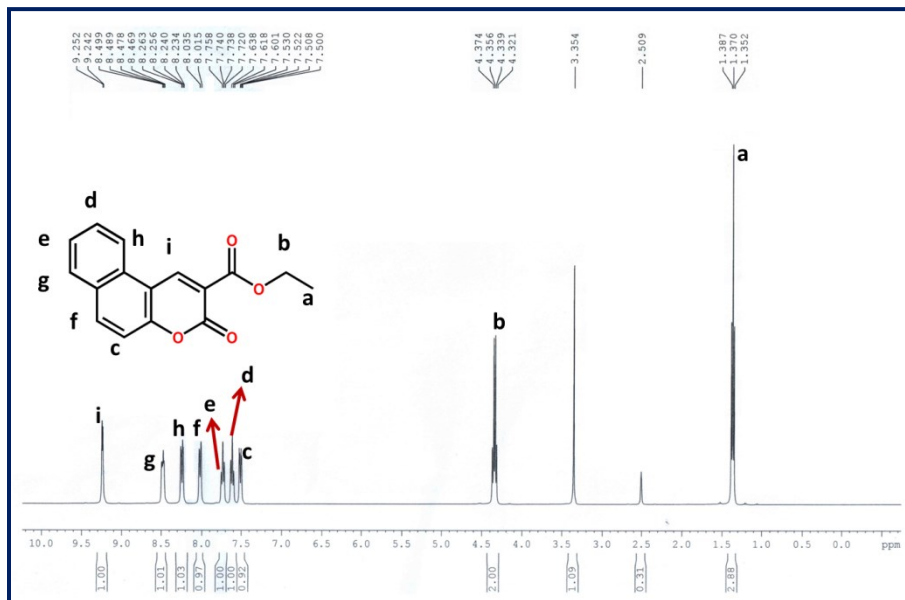


Fig. S1. ¹H NMR spectrum of (**L1**) in DMSO-*d*₆.

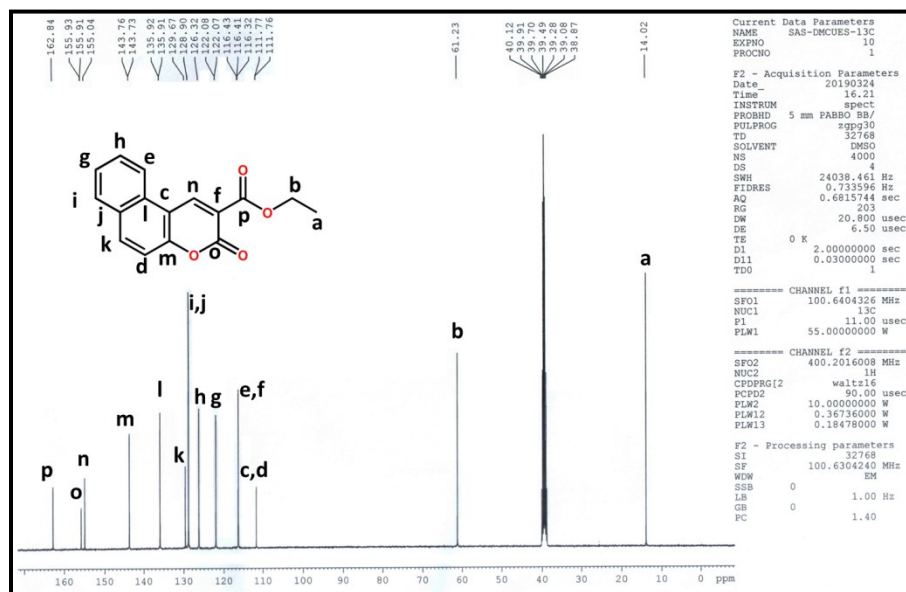


Fig. S2. ¹³C NMR spectrum of (**L1**) in DMSO-*d*₆.

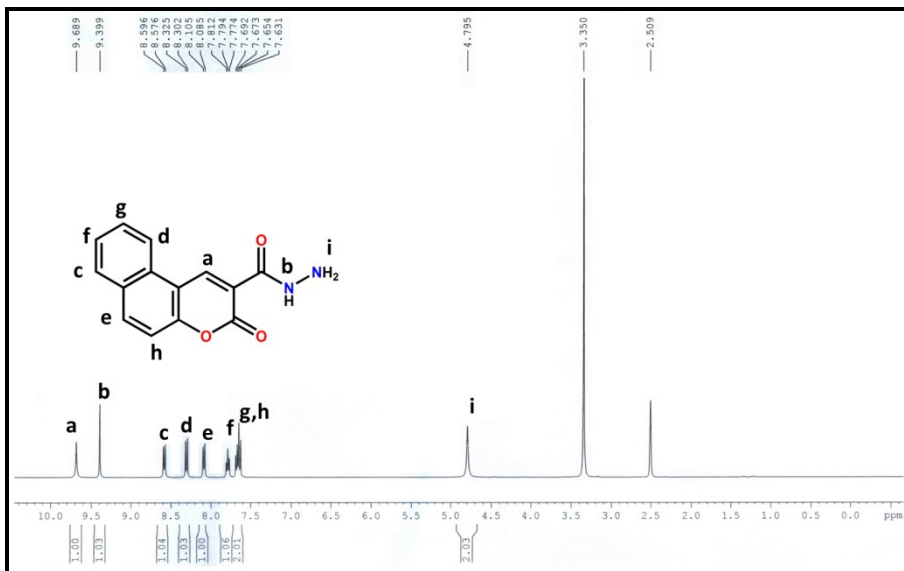


Fig. S3. ¹H NMR spectrum of BCM in DMSO-*d*₆.

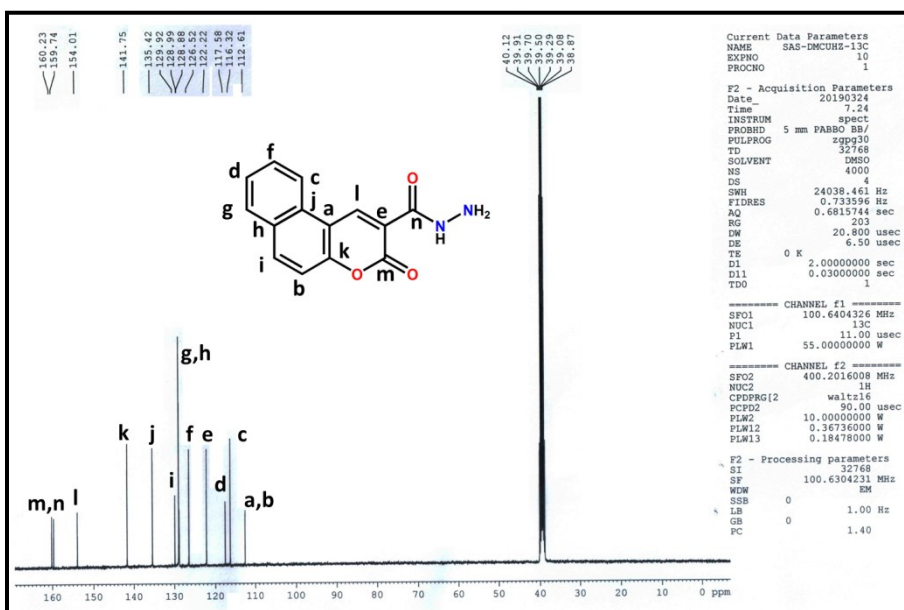


Fig. S4. ¹³C NMR spectrum of BCM in DMSO-*d*₆.

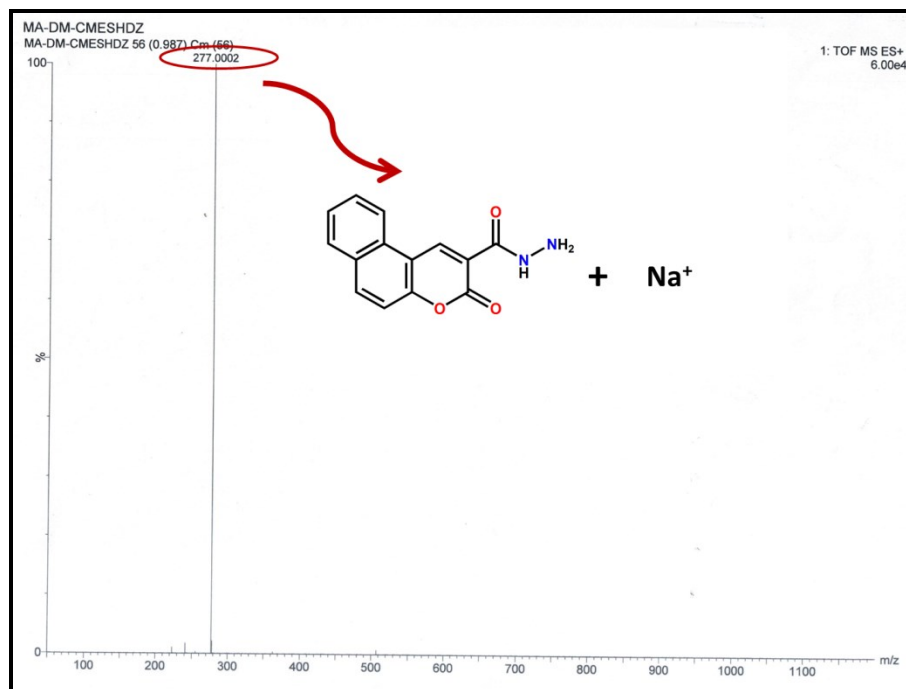


Fig. S5. Mass spectrum of BCM.

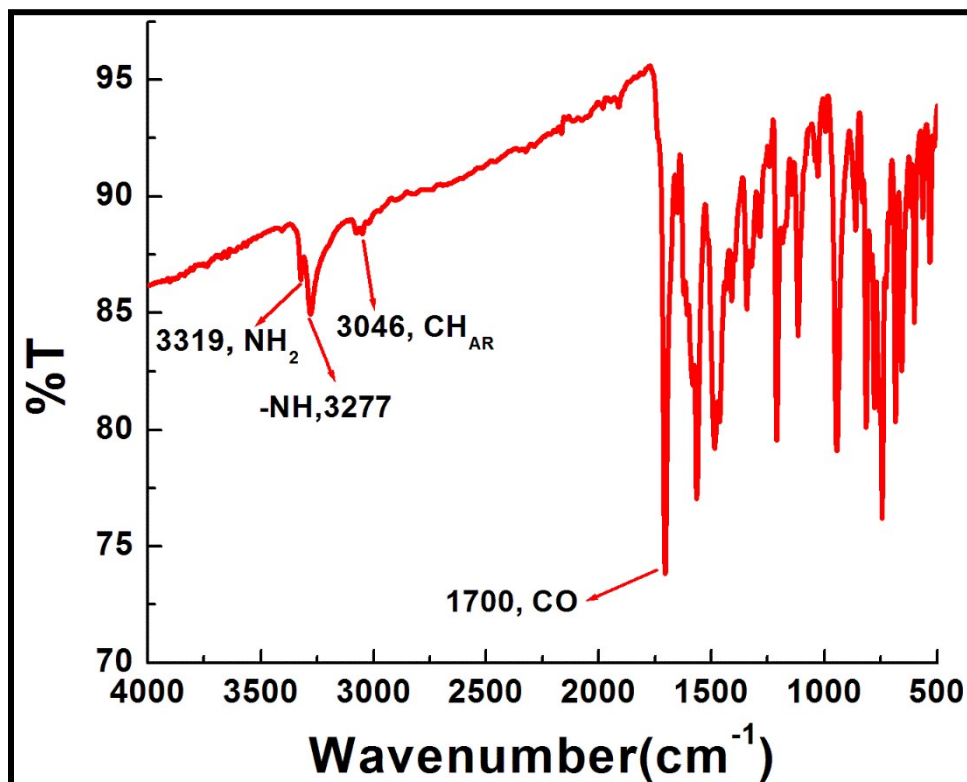


Fig. S6. IR spectra of BCM

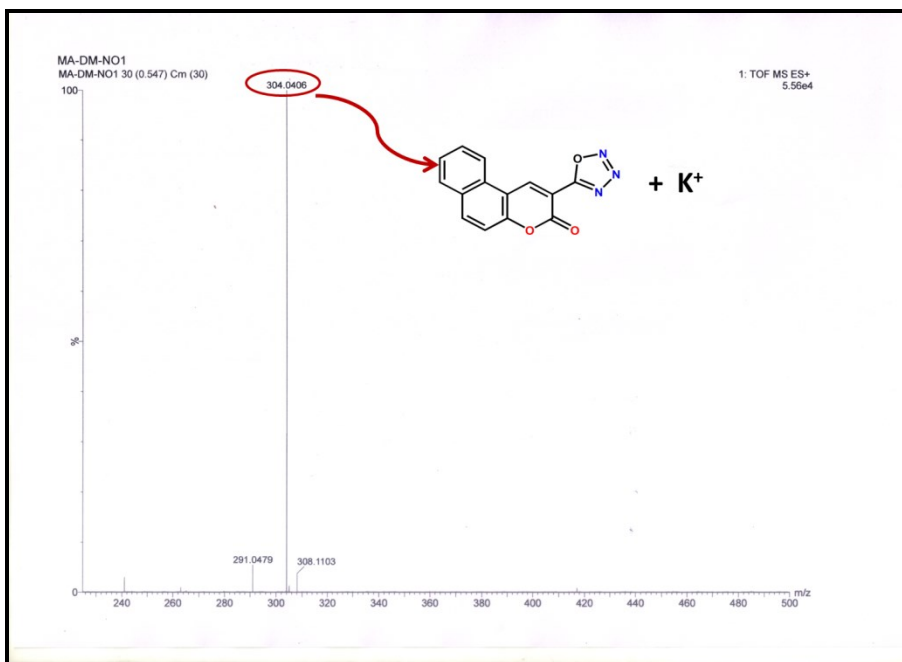


Fig. S7. Mass spectrum of BCM-NO

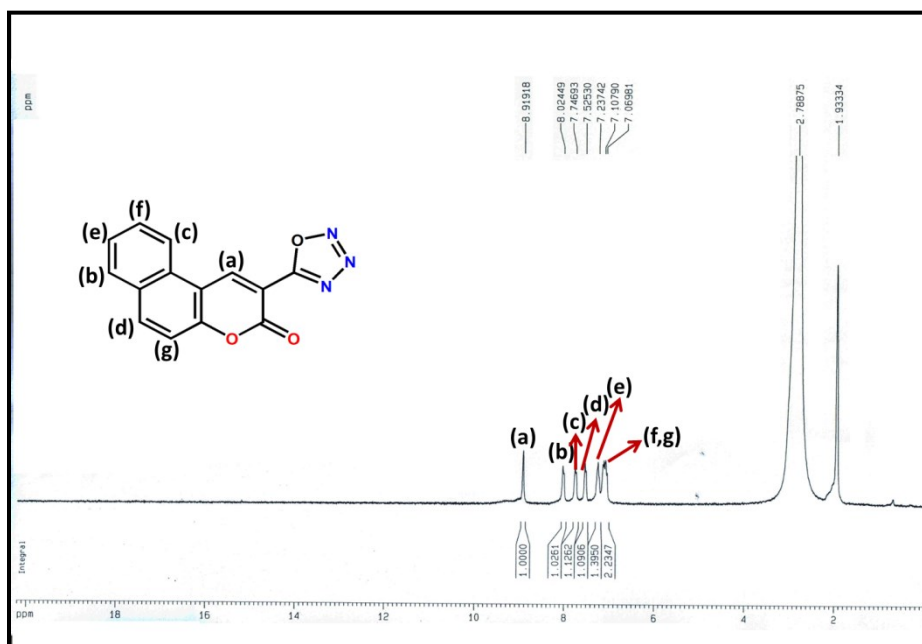


Fig. S8. ¹H NMR spectrum of BCM-NO in MeCN (minimum DMSO-*d*₆).

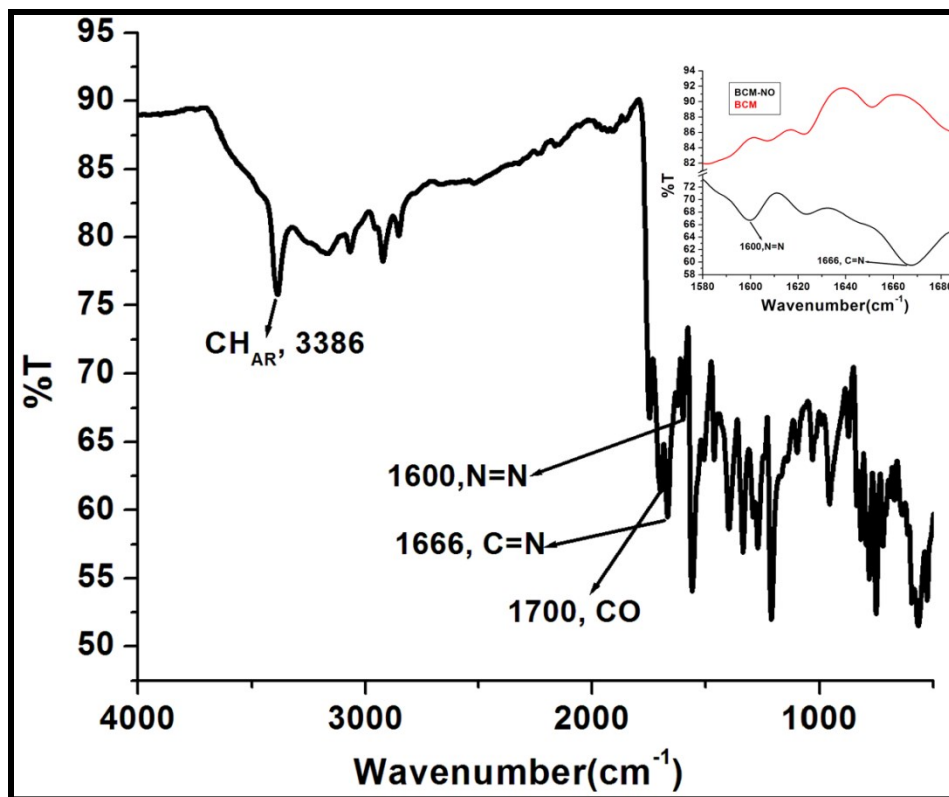


Fig. S9. IR of BCM-NO.

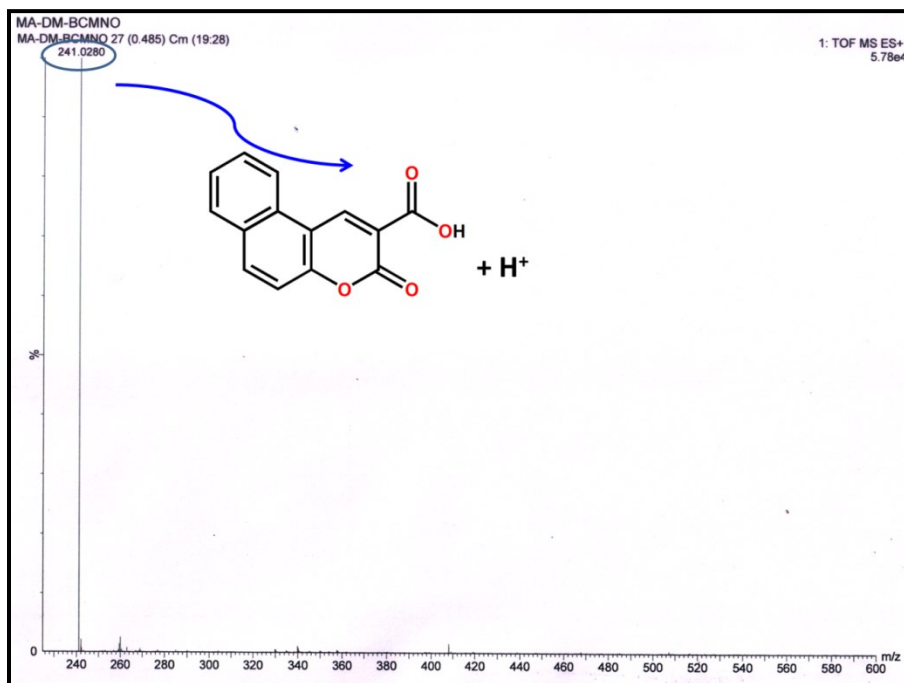


Fig. S10. Mass spectrum of BCM-NO after long time (acid product)

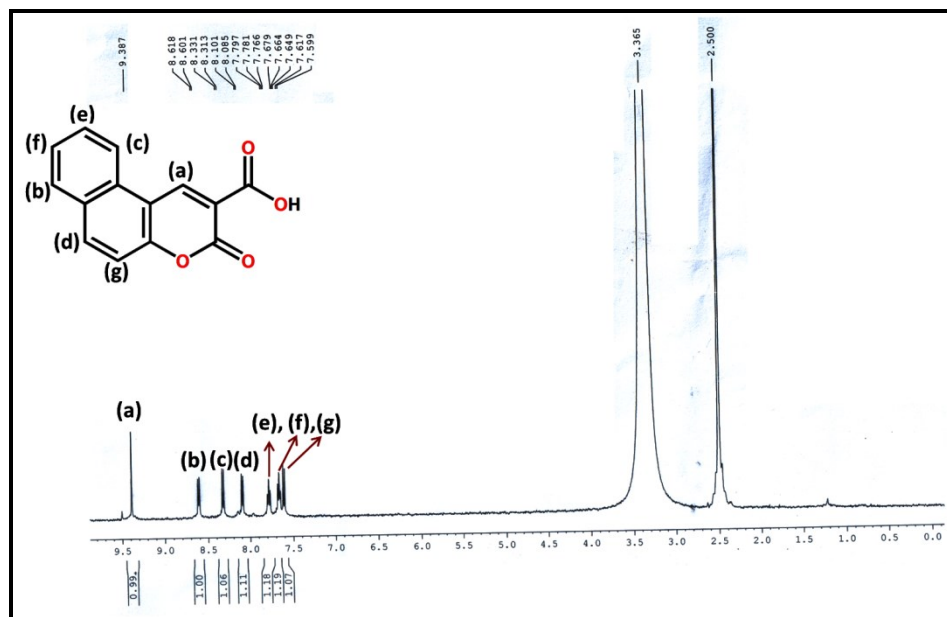


Fig. S11. ¹H NMR spectrum of BCM-NO after long time (acid product) in DMSO-d₆.

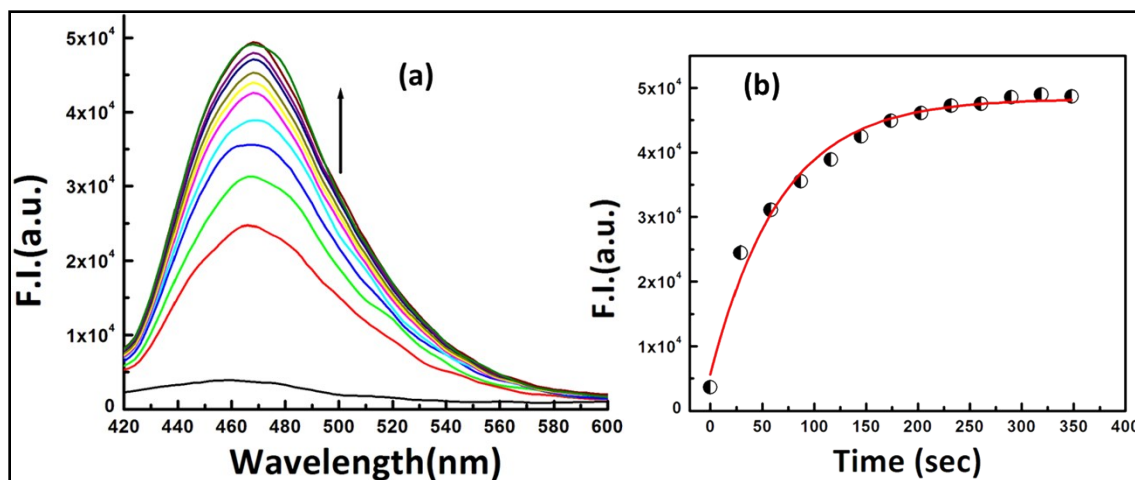


Fig. S12(a) Time-dependent fluorescence response and (b) corresponding growth curve for [BCM] = 5.0 μM and [NO] = 5.0 μM at 15 °C.

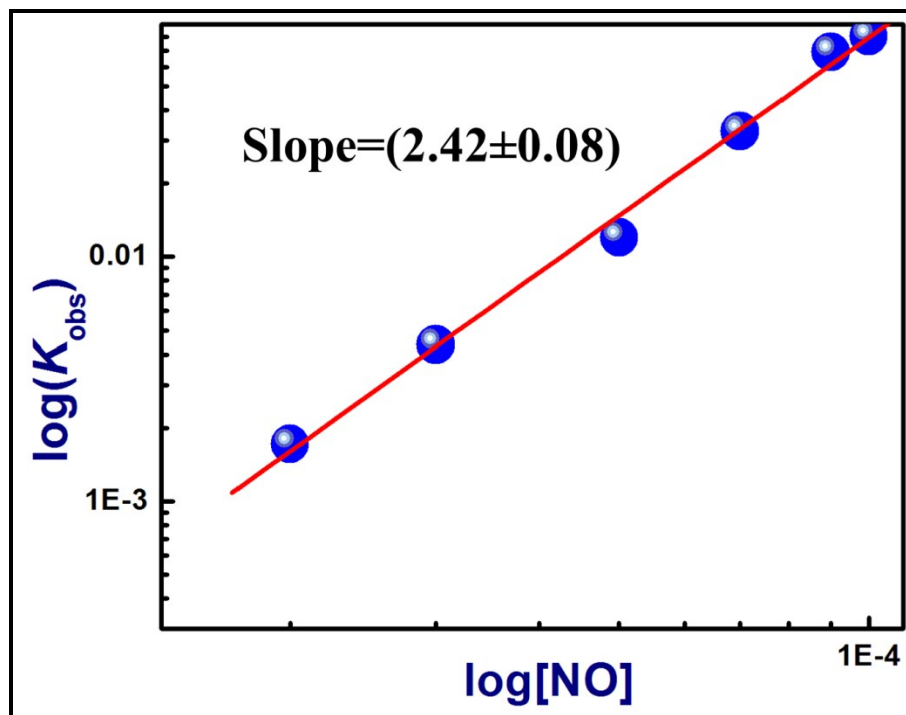


Fig. S13. Plot of $\log(k_{\text{obs}})$ vs. $\log [\text{NO}]$.

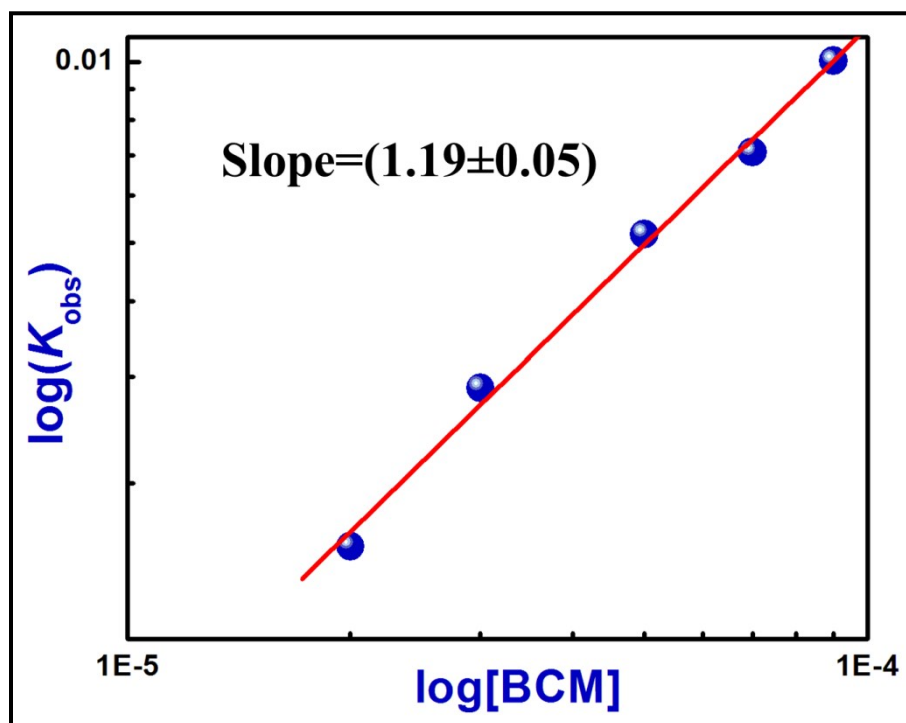


Fig. S14. Plot of $\log(k_{\text{obs}})$ vs. $\log [\text{BCM}]$.

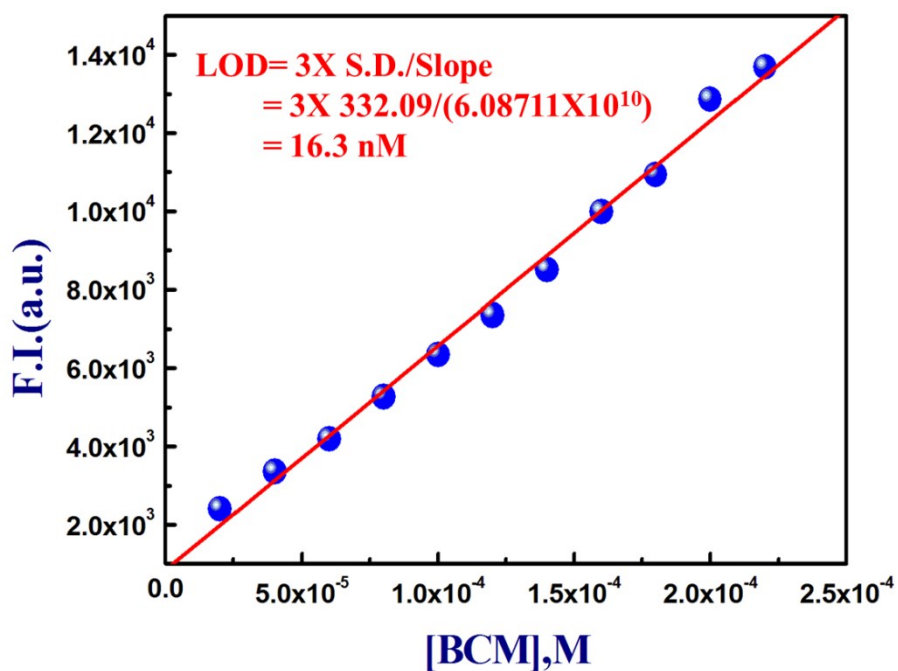


Fig. S15. LOD of BCM + NO.

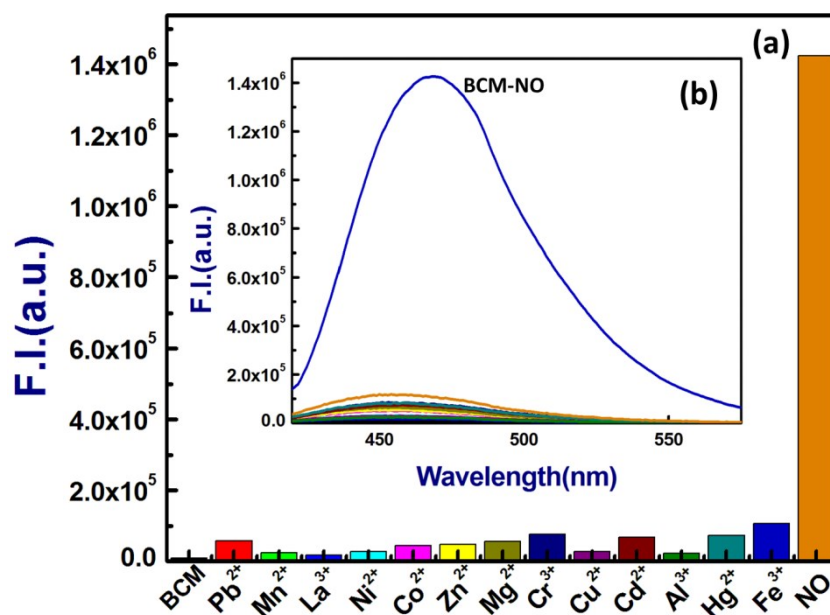


Fig. S16. (a) Bar chart illustrating fluorescence response of BCM to different cations at 470 nm ($\lambda_{ex} = 410 \text{ nm}$) in HEPES buffer pH 7.0; BCM = 20 μM , $M^{n+} = 50 \mu\text{M}$. (b) spectral responses.

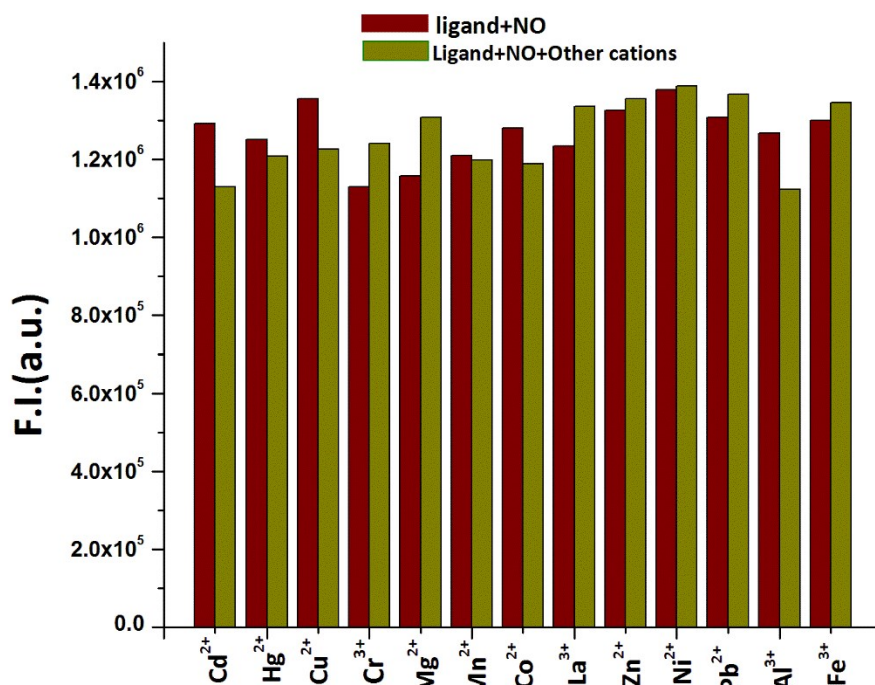


Fig. S17. Bar chart illustrating fluorescence response of BCM at 470 nm ($\lambda_{ex} = 410$ nm) towards NO in presence of different cations in HEPES buffer pH 7.0; BCM = 20 μ M, $M^{n+} = 50$ μ M.

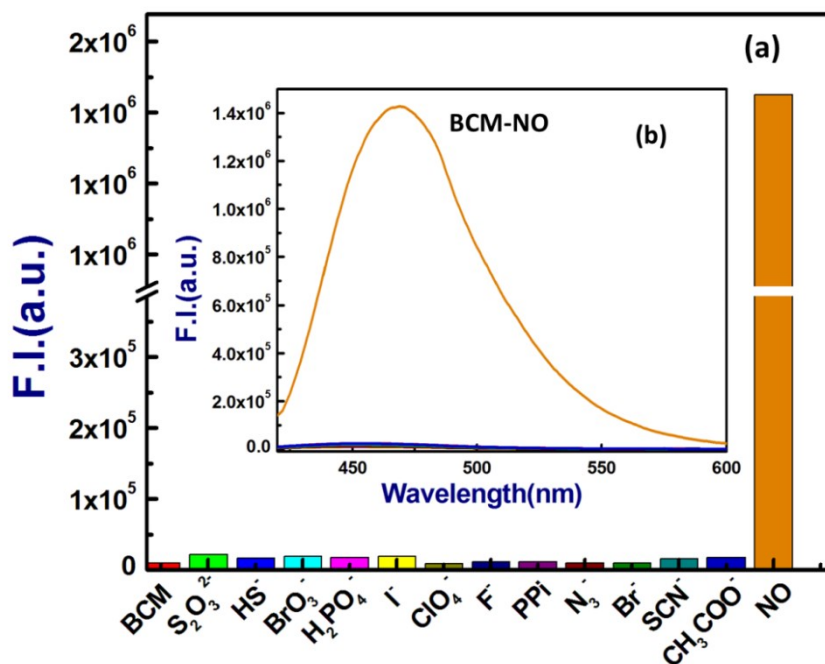


Fig. S18. (a) Bar chart illustrating fluorescence response of BCM to different anions at 470 nm ($\lambda_{ex} = 410$ nm) in HEPES buffer pH 7.0; BCM = 20 μ M, $X^{n-} = 50$ μ M. (b) spectral responses.

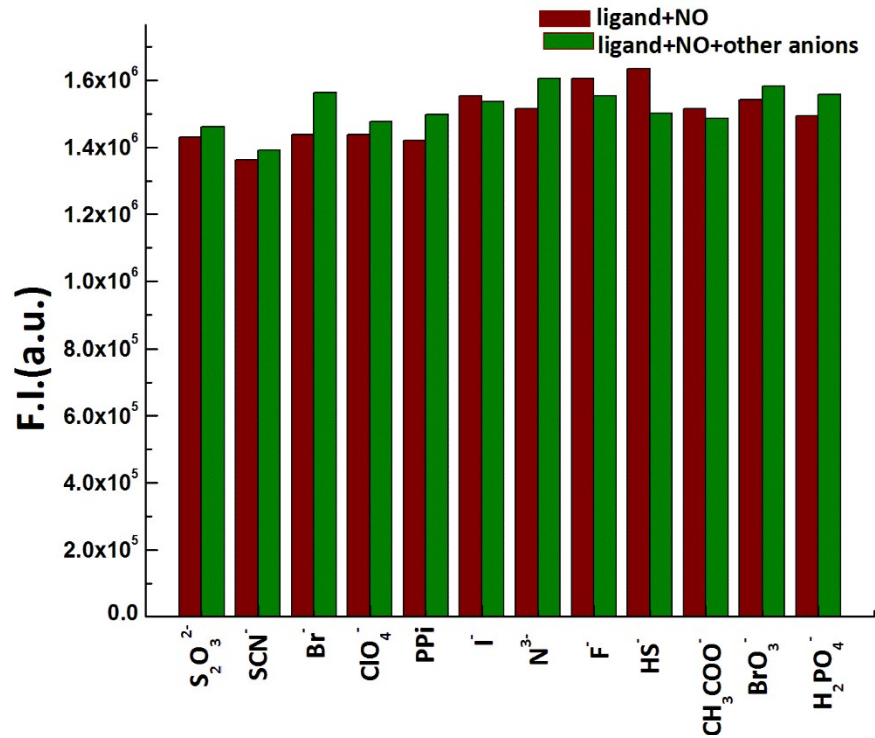


Fig. S19. Bar chart illustrating fluorescence response of BCM at 470 nm ($\lambda_{\text{ex}} = 410$ nm) towards NO in presence of different anions in HEPES buffer pH 7.0; BCM = 20 μM , $\text{X}^{\text{n-}} = 50$ μM .

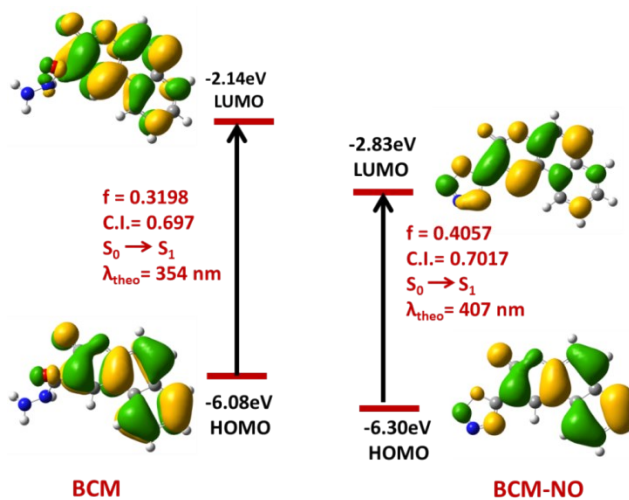


Fig. S20. Frontier molecular orbitals of BCM and BCM-NO in UV-vis absorption.

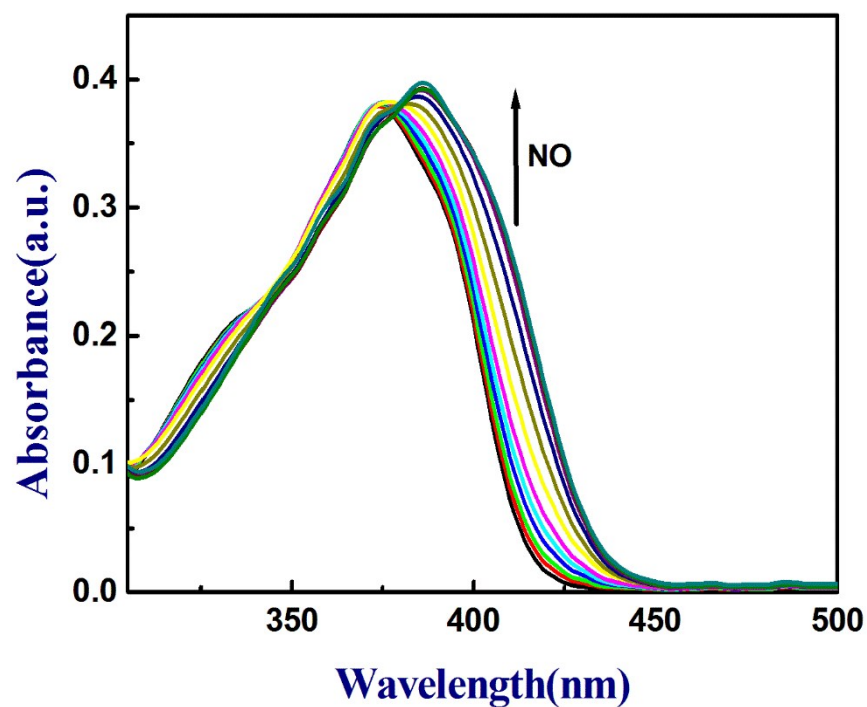


Fig. S21. UV response of BCM towards nitric oxide.

Table S1. Some selected geometrical parameters (bond lengths and bond angles) of **BCM** in ground state calculated at B3LYP/6-31G (d,p) Levels.

Bond Lengths (Å)		Bond Angles (°)	
O21-C1	1.40	O22-C1-C5	127.16
C1-O22	1.20	C1-C5-C23	117.27
C5-C23	1.51	C5-C23-O24	122.09
C23-O24	1.21	O24-C23-N25	125.47
C23-N25	1.38	C23-N25-N26	119.59

Table S2. Some selected geometrical parameters (bond lengths and bond angles) of **BCM-NO** in ground state calculated at B3LYP/6-31G (d,p) Levels.

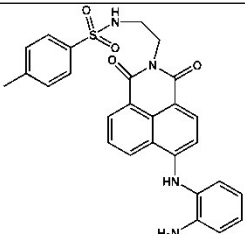
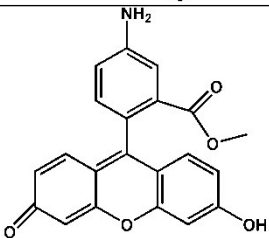
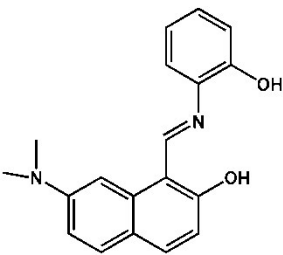
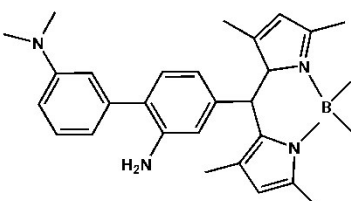
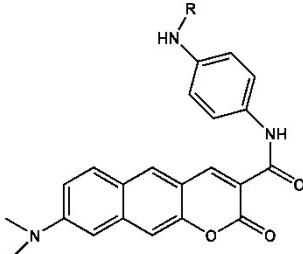
Bond Lengths (Å)		Bond Angles (°)	
O21-C1	1.40	O21-C1-O22	117.61
C1-O22	1.20	O22-C1-C5	127.89
C1-C5	1.46	C5-C23-O24	122.79
C5-C23	1.45	C23-O24-N25	104.10
C23-O24	1.32	O24-N25-N26	106.54
O24-N25	1.43	N25-N26-N27	112.77
N25-N26	1.25	C23-N27-N26	104.42
N26-N27	1.36		
N27-C23	1.31		

Table S3. Vertical excitation energy and oscillator strength (f_{cal}) of low-lying excited singlet states obtained from TDDFT// B3LYP/6-31G(d,p) calculations of **BCM** which is matched with the experimental one.

Electronic transition	Composition	Excitation energy	Oscillator strength (f_{cal})	CI	λ_{exp} (nm)
$S_0 \rightarrow S_1$	HOMO→LUMO (66 →67)	3.499eV (354.29nm)	0.3198	0.69768	374

Table S4. Vertical excitation energy and oscillator strength (f_{cal}) of low-lying excited singlet states obtained from TDDFT// B3LYP/6-31G(d,p) calculations of **BCM-NO** which is matched with the experimental one.

Electronic transition	Composition	Excitation energy	Oscillator strength (f_{cal})	CI	λ_{exp} (nm)
$S_0 \rightarrow S_1$	HOMO→LUMO (68 →69)	3.043eV (407.42nm)	0.4057	0.70177	386

Serial no.	Structure of probe	LOD	fold	medium	mechanism	Emission wavelength	kinetics	Reference
1.		3.3nM	22	PBS buffer	OPD- based	538nm	Not done	<i>ACS Sens.</i> 2018,3, 11, 2311
2.		44nM	–	Hepes buffer	De-amination	524nm	Not done	<i>Inorg. Chem.</i> 2012, 51, 5400
3.		97.81 nM	7.5	PBS Buffer (5%DMSO +0.2% Triton X-100)	Breaking of Schiff base	590nm	Not done	<i>Chem. Commun.</i> , 2018, 54, 13491
4.		30nM	5	Ethanol + PBS buffer 1:1	Through diazonium intermediate	518nm	Not done	<i>Chem. Commun.</i> , 2014, 50, 7499
5.		37nM	–	PBS+10% MeCN	N-Nitrosation	613nm	Not done	<i>Chem. Sci.</i> , 2017, 8, 4533

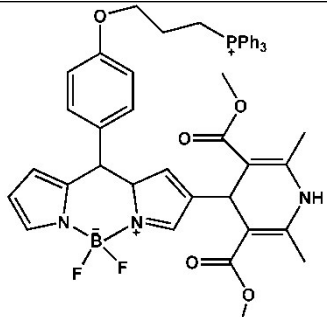
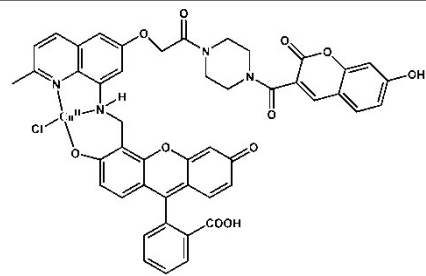
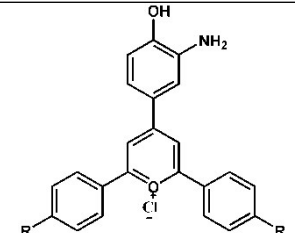
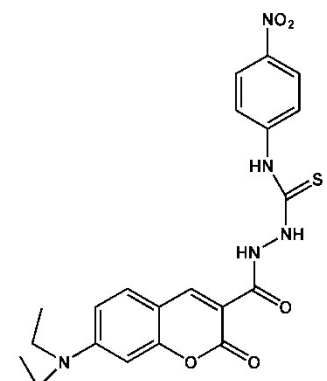
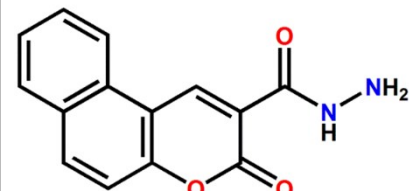
6.		25nM	63	PBS buffer	Hanstch ester synthesis	525nm	Not done	Talanta 176 (2018) 382
7.		21nM	11	PBS buffer	Metal based sensor	522nm	Not done	J. Mater. Chem. B, 2017, 5, 8929
8.		2.1 μM	83	Aerated H ₂ O	Deamination	550nm	Not done	Chem. Commun., 2014, 50, 3579
9.		47.6 nM	5	DMSO+ Hepes buffer 3:7	1,3,4-oxadiazole formation	475nm	Not done	ACS Sens. 2019, 4,2, 309
10.		16nM	123	Hepes buffer	1,2,3,4 oxatriazole	470nm	Done	This work

Table S5. Comparison table of some previously reported nitric oxide probes.

Physical Instrumentations. For analysis, the IR spectra of the compound within 400-4000 cm^{-1} has been obtained using IR 750 series-II FTIR (Nicolet Magna) spectrophotometer on solid KBr discs. ^1H and ^{13}C NMR spectra were recorded taking solvent DMSO- d_6 in a Bruker 300 MHz and 400 MHz instrument using trimethylsilane ($\delta = 0$) as an internal standard. To record ESI-MS $^+$ (m/z) spectra the mass spectrometer having Model: QTOF Micro YA263 was used. pH was maintained through-out the study using a digital pH meter (Model: Systronics 335, India) in the pH range 2–11 which was already calibrated using buffers of pH 4, 7 and 10. For all the fluorescence studies, a PTI (Model QM-40) spectro-fluorimeter was used and UV-vis spectra were recorded on an Agilent 8453 Diode-array spectrophotometer.

Kinetic Studies. We have performed the kinetic studies of NO detection maintaining the pseudofirst-order conditions taking fixed 5 μM BCM (minor component) and varying the NO concentration in the range 20 μM and 100 μM at pH 7.0, at 15 $^\circ\text{C}$. The rate of the reaction also depends on the [BCM] which is evaluated keeping NO (5 μM) as minor component. The plot of $\log k_{\text{obs}}$ vs. $\log[\text{BCM}]$ and $\log k_{\text{obs}}$ vs. $\log[\text{NO}]$ shows about the first order and second order dependency of reaction upon [BCM] and [NO] respectively.

Stock solution preparation for photophysical studies. The stock solution of the probe BCM was prepared in a 10 ml of volumetric flask of 1.0×10^{-3} M in minimum DMF adjusted with CH_3CN . For Nitric Oxide solution preparation, Nitric Oxide gas (purified previously by passing through solid NaOH pellets) was purged for 15 mins in a sealed vial containing deoxygenated deionized water.⁵¹ This solution gives the NO concentration 1.74×10^{-3} M. For nitroxyl (HNO), Angeli's salt was taken.⁵² By adopting the reported literature, $\cdot\text{OH}$ and ONOO^- solutions were prepared.⁵³ The solutions of different cations, anions and biological species were prepared in H_2O . Throughout the experiments, a 10.0 mM HEPES buffer was taken maintaining pH 7.0 and ionic strength at 0.10 M (NaCl). In this work, 20 μM of the probe BCM, was added in a 2.5 ml of the 10.0 mM HEPES buffer upon which, nitric oxide solution (~ 40 μM) was added incrementally in a regular time interval and the fluorescence spectra were recorded in each case with slits 2 X 2 nm, $\lambda_{\text{ex}}=410$ nm.

Calculation of Detection Limit (LOD). For the determination of analytical limit of detection, we have adapted the 3σ method, narrated below:

$$\text{LOD} = 3 \times S_d / S$$

S_d denotes the standard deviation obtained from the intercept of the plot of fluorescence intensity (F.I.) vs. [BCM] where, S represents the slope found from the linear plot of F.I. vs [NO].

Computational Details. For theoretical investigation we have performed the computational data analysis by DFT method⁵⁴ which is incorporated with the conductor-like polarizable continuum model (CPCM).⁵⁵⁻⁵⁷ In this study, the Becke's hybrid function⁵⁸ with the Lee-Yang-Parr (LYP) correlation function⁵⁹ are also utilized. To get the fully optimized geometry of BCM and BCM-NO we have taken 6-31G(d,p) basis set and for electron density plots Gauss View 5.1 software was used. The absorption spectra of both the compound were also calculated by TD-DFT method using the 6-31G(d,p) basis set. All the related calculations were made applying Gaussian 09W software package⁵¹⁰ and for the calculation of molecular orbital contributions we have used Gauss Sum 2.1 programme.⁵¹¹

Cell culture and Cytotoxicity Assay. Human cancer cell line A375 (malignant skin melanoma) and Raw 264.7 murine macrophages cells were grown in DMEM (Dulbecco's modified Eagle's) medium furnished with 10% FBS and 1% antibiotic at 37 $^\circ\text{C}$ with 5% CO_2 .⁵¹² We have investigated the cell viability of the probe BCM in A375 and

Raw 264.7 cells with the gradually incremented concentration (ranging from 10–100 $\mu\text{M}/\text{mL}$) of BCM for 24 h by the MTT assay.^{S13}

Cell Incubation, Imaging and Flow Cytometry Analysis. Cell imaging for exogenous and endogenous NO monitoring were carried out by exploiting reported method^{S12,S13} with A375 and Raw 264.7 cells respectively. Exogenously, A375 cells were incubated on a glass coverslip, followed by the treatment with DEA-NONOate (NO donor, 2 μM , 5 μM and 10 μM) for 30 min. Then the coverslip was washed with 1X PBS for three times and afterwards treated with BCM for 30 min. Endogenously, Raw 264.7 cells were co-stimulated with or without LPS (1.0 mg/ mL) and IFN- γ (1000 U/mL) for 6h and furthermore incubated with BCM (5 μM) for 30 min and with or without NO scavenger PTIO (2-phenyl-4,4,5,5-tetramethylimidazoline-1-oxyl 3-oxide). The cellular fluorescence was accompanied only through NO generation which was assured by NO scavenger PTIO (2-Phenyl-4,4,5,5-tetramethylimidazoline-1-oxyl-3-oxide) treatment. Then the live cell imaging by using fluorescence microscope (Carl Zeiss, Germany) was furnished. Next, 1×10^6 Raw 264.7 cells were seeded in a T25 flask (BD Falcon) maintaining 37 °C. Again the cells were incubated with our probe BCM for 30 min, afterwards, co-stimulated with or without LPS and IFN- γ for 6 h and also taking the NO scavenger PTIO (2-phenyl-4,4,5,5-tetramethylimidazoline-1-oxyl 3-oxide) live cell images were collected. Next, treated and untreated control cells were washed with ice-cold 1 \times PBS which was resuspended in 500 μL of binding buffer and the flow cytometric analysis was carried out with FACS LSR (Becton Dickinson). The Flow cytometry analysis was performed by using Flowing Software, version 2.5.1.

References:

- S1. Š. Mesároš, S. Grunfeld, A. Mesárošová, D. Bustin and T. Malinski, *Anal. Chim. Acta*, 1997, 339, 265–270.
- S2. A. T. Wrobel, T. C. Johnstone, A. D. Liang, S. J. Lippard and P. A. Rivera-Fuentes, *J. Am. Chem. Soc.*, 2014, 136, 4697–4705.
- S3. M. Grätzel, S. Taniguchi and A. Henglein, *Ber. Bunsen-Ges. Phys. Chem.*, 1970, 74, 488–492.
- S4. R. G. Parr and W. Yang, *Density Functional Theory of Atoms and Molecules*, Oxford University Press, Oxford, 1989.
- S5. V. Barone and M. Cossi, *J. Phys. Chem. A*, 1998, 102, 1995–2001.
- S6. V. Barone and M. Cossi, *J. Chem. Phys.*, 2001, 115, 4708–4717.
- S7. M. Cossi, N. Rega, G. Scalmani and V. Barone, *J. Comput. Chem.*, 2003, 24, 669–681.
- S8. A. D. Becke, Density-functional thermochemistry. III. The role of exact exchange. *J. Chem. Phys.*, 1993, 98, 5648–5652.
- S9. C. Lee, W. Yang and R. G. Parr, *Phys. Rev. B: Condens. Matter Mater. Phys.*, 1988, 37, 785–789.
- S10. M. J. Frisch, G. W. Trucks, H. B. Schlegel, G. E. Scuseria, M. A. Robb, J. R. Cheeseman, G. Scalmani, V. Barone, B. Mennucci, G. A. Petersson, H. Nakatsuji, M. Caricato, X. Li, H. P. Hratchian, A. F. Izmaylov, J. Bloino, G. Zheng, J. L. Sonnenberg, M. Hada, M. Ehara, K. Toyota, R. Fukuda, J. Hasegawa, M. Ishida, T. Nakajima, Y. Honda, O. Kitao, H. Nakai, T. Vreven, J. A. Montgomery Jr., J. E. Peralta, F. Ogliaro, M. Bearpark, J. J. Heyd, E. Brothers, K. N. Kudin, V. N. Staroverov, R. Kobayashi, J. Normand, K. Raghavachari, A. Rendell, J. C. Burant, S. S. Iyengar, J. Tomasi, M. Cossi, N. Rega, J. M. Millam, M. Klene, J. E. Knox, J. B. Cross, V. Bakken, C. Adamo, J. Jaramillo, R. Gomperts, R. E. Stratmann, O. Yazyev, A. J. Austin, R. Cammi, C. Pomelli, J. W. Ochterski, R. L. Martin, K. Morokuma, V. G. Zakrzewski, G. A. Voth, P. Salvador, J. J. Dannenberg, S. Dapprich, A. D. Daniels, Ö. Farkas, J. B. Foresman, J. V. Ortiz, J. Cioslowski and D. J. Fox, *Gaussian 09*, (Revision A.1), Gaussian, Inc., Wallingford, CT, 2009.
- S11. N. M. O’Boyle, A. L. Tenderholt, K. M. Langner, *J. Comput. Chem.*, 2008, 29, 839–845.
- S12. A. S. M. Islam, R. Bhowmick, B. C. Garain, A. Katarkar and M. Ali, *J. Org. Chem.*, 2018, 83, 13287–13295.
- S13. A. S. M. Islam, R. Bhowmick, K. Pal, A. Katarkar, K. Chaudhuri and M. Ali, *Inorg. Chem.* 2017, 56, 4324–4331.